Publ. Astron. Soc. Japan **41**, 345–372 (1989)

The Large Area Counter on Ginga

Martin J. L. TURNER and Huw D. THOMAS*

X-Ray Astronomy Group, Department of Physics, University of Leicester, University Road, Leicester, LE1 7RH, U.K.

Bruce E. PATCHETT and Douglas H. READING

Space and Astrophysics Group, Rutherford Appleton Laboratory, Didcot, OX11 0QX, U.K.

Kazuo MAKISHIMA and Takaya OHASHI

Department of Physics, The University of Tokyo, 3–1, Hongo 7-chome, Bunkyo-ku, Tokyo 113

Tadayasu DOTANI, Kiyoshi HAYASHIDA, Hajime INOUE, Hideji KONDO, Katsuji KOYAMA,† Kazuhisa MITSUDA, Yoshiaki OGAWARA, and Shirou TAKANO†

Institute of Space and Astronautical Science, 1–1, Yoshinodai 3-chome, Sagamihara-shi, Kanagawa 229

Hisamitsu AWAKI and Yuzuru TAWARA

Department of Astrophysics, School of Science, Nagoya University, Furo-cho, Chikusa-ku, Nagoya 464–01

and

Norio NAKAMURA

National Laboratory for High Energy Physics, Tsukuba, Ibaraki 300–32

(Received 1988 September 13; accepted 1989 February 23)

Abstract

The large-area counter on the third Japanese X-ray astronomy satellite Ginga is described. It comprises eight multi-cell proportional counters with a total effective area of 4000 cm^2, covering the energy range 1.5 to 37 keV. The energy resolution is 18% at 6 keV, and scales as $E^{-0.5}$ over the full energy range. The field of view of the collimator is elliptical ($1.^\circ1 \times 2.^\circ0$

* Present address: British Aerospace, Stevenage, Herts, U.K.

† Present address: Department of Astrophysics, School of Science, Nagoya University, Furo-cho, Chikusa-ku, Nagoya 464–01.

FWHM), giving a 3σ confusion limit of about 0.2 mCrab. Shielding against the diffuse cosmic X-ray background, and anticoincidence background rejection techniques give an in-orbit background of 3.5×10^{-4} counts $cm^{-2} s^{-1} keV^{-1}$. The LAC is able to measure the spectrum and study the time variability of X-ray sources down to about 0.2-mCrab intensity. The ultimate time resolution is 1 ms, and the large area gives significant counting rates from bright sources in time bins of a few ms long.

Key words: Crab Nebula; Instruments; X-ray astronomy.

1. Introduction

The third Japanese X-ray astronomy satellite Ginga (ASTRO-C) was launched on a Mu-3S-II-3 rocket from the Kagoshima Space Centre on February 5th 1987 at 06:30 UT. The satellite carries a payload comprising three instruments: the large area counter (LAC), the all sky monitor (ASM) and the gamma-ray burst detector (GBD). A brief description of the satellite and its payload has been given by Makino and the ASTRO-C team (1987). The LAC is the primary instrument on Ginga and its main objectives include: the study of AGN; the study of fast time variability in compact galactic sources; and spectral surveys in the medium energy band of various classes of faint X-ray sources, ranging from stars to galaxies. With its large effective area ($4000\,cm^2$) and low internal background, the LAC is the most sensitive instrument in this energy band yet in orbit. It is capable of measuring the spectra of cosmic X-ray sources of intensity as low as $4 \times 10^{-12}\,erg\,cm^{-2}\,s^{-1}$ (2–10 keV) or about 0.2 mCrab. For bright galactic sources time resolution, with significant count rates, can be as small as a few milliseconds.

The LAC was designed and built by a single scientific team whose members came from the following research groups: in the United Kingdom, the X-ray Astronomy group of the Physics Department, University of Leicester; and the Space and Astronomy group of the Rutherford Appleton Laboratory: in Japan, the X-ray Astronomy groups of ISAS; the Physics Department, University of Tokyo; and the Astrophysics Department, Nagoya University. The construction of the LAC proportional counters, together with their front end electronics, calibration system, and harness, was carried out in the United Kingdom; while the high-voltage supplies, the main electronics and data conditioning system were produced in Japan. The integration and testing of the complete LAC, as well as some of the environmental testing of individual LAC modules, took place in Japan.

This paper describes the LAC instrument and its operation, together with its design, construction and calibration. The background and sensitivity of the LAC are also briefly discussed. A detailed study of the LAC internal background and its estimation is given in the following paper (Hayashida et al. 1989).

2. The LAC Instrument

The LAC instrument is shown in figure 1. It consists of eight identical sealed collimated proportional counters. The counters are filled with argon (75%), xenon

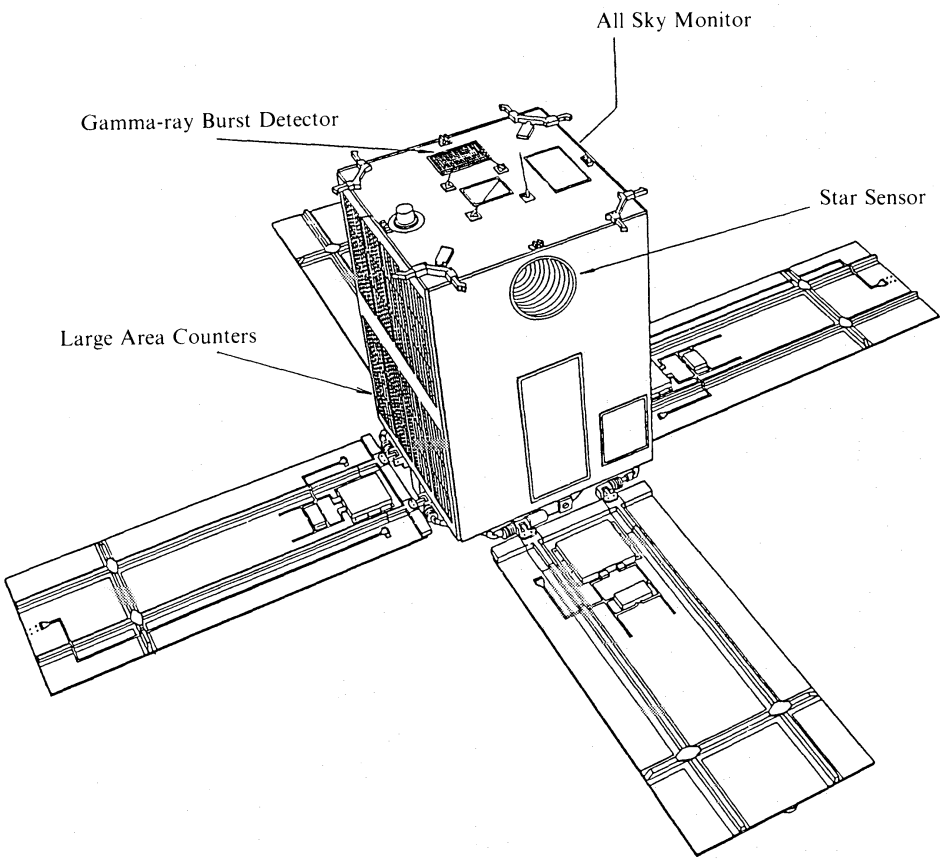

Fig. 1. The LAC instrument showing the eight coaligned collimated proportional counters mounted on the Y face of the spacecraft.

(20%) and carbon dioxide (5%) at the pressure of 1.86 atm (at 273 K). The beryllium entrance window is 62 μm thick and the active depth of the counters is 3.9 cm. All the collimators have the same field of view ($1^\circ \times 2^\circ$ FWHM), and the counters, mounted on one side panel of the spacecraft, are coaligned. The LAC can be directed to any point on the celestial sphere (outside the sun constraint) by manoeuvring and slewing the spacecraft. Figure 2 shows the elliptical field of view of the collimator and its relationship to the spacecraft axes. The spacecraft uses a momentum wheel to control movement in the X-Y plane (slew) and three magneto-torquers to manoeuvre and stabilize the Z axis. The attitude is measured and controlled using four gyros and two star trackers in a closed loop system. Table 1 gives the manoeuvring constraints and attitude stability as measured in orbit. The main constraint requires the angle between the sun and the LAC to be between 50° and 130°. Recent practice has been to restrict this angle to a value greater than 90° in order to avoid occasional solar contamination of the observations.

The energy range 0 to 37 keV is divided into 64 equal energy channels, the upper 32 channels are combined in pairs for storage and transmission. Various data compression modes can be selected according to the desired time resolution, details of the available modes are given in table 2. The satellite is in contact with the ground station on five of the fifteen orbits in an observing day; manoeuvres and commands

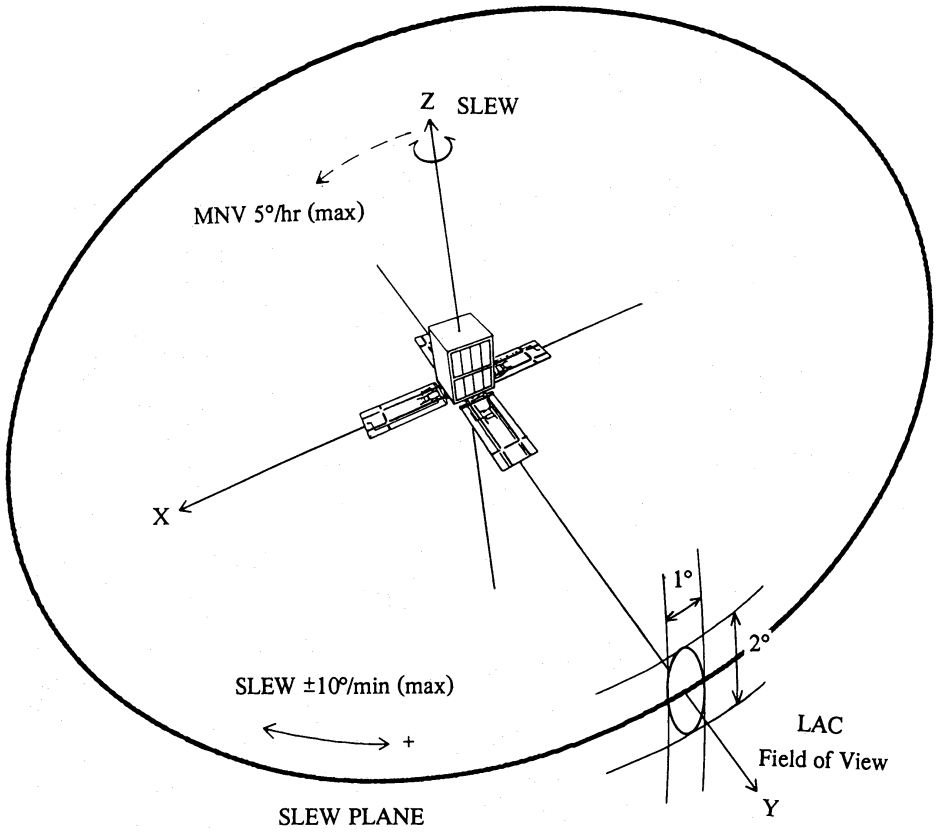

Fig. 2. The collimator field of view (FWHM) and the satellite three axes. The stability of the attitude is better in the Y direction than in the Z direction and hence the field of view has an elliptical shape. The Y direction is in the slew plane of the spacecraft.

Table 1. Manoeuvring constraints and attitude stability.

Item	Constraint
Sun angle*	Power constraint: 50° to 130°
	Solar X-ray constraint: >90°
Manoeuvre	5° hr^{-1} (typically)
Slew	14° min^{-1}
Stability	0.1° d^{-1} (typically)

* Angle between the LAC f.o.v. and the Sun.

are programmed on these passes. Data are stored during the orbit in the 40-Mbit bubble memory data recorder (BDR) for transmission to the ground station. For the ten noncontact orbits data continue to be recorded until next ground contact. In this case the mode and recording rate are selected so that the BDR does not fill prematurely. Table 3 gives the capacity of the BDR for the various recording rates.

The internal background varies by a factor of two through the observing day and secularly by 25% with a period of 37 days, due to the slight eccentricity of the orbit ($e=0.01$). The LAC has no simultaneous background measurement capability so a typical observation requires one day on the source and an adjacent day to measure

Table 2. Time resolution for each data mode.

Mode	PH channel	Bit rate			Note
		High	Medium	Low	
MPC1	48	500 ms	4 s	16 s	8 detectors by 2 layers
MPC2	48	62.5 ms	500 ms	2 s	4 detectors combined
MPC3	12	7.8 ms	62.5 ms	250 ms	8 detectors combined
PC-H		1.9 ms	15.6 ms	62.5 ms	4 detectors combined
-L		0.98 ms	7.8 ms	31.3 ms	4 detectors combined

Table 3. BDR recording time.

Bit rate	Recording time
High (16 kbps)	43 min
Medium (2 kbps)	5 h 42 min
Low (512 bps)	22 h 45 min

the background. The period of lowest and most stable background occurs during the ten noncontact orbits. Background measurement and estimation are discussed in section 5.

3. Technical Description

3.1. The Proportional Counters

3.1.1. Design considerations

The main objectives in the design of the LAC were to achieve as large an effective area as possible within the constraints of mass and volume imposed by the spacecraft, and to have a very low internal background; the five year planned mission lifetime also imposed a requirement for high reliability. The philosophy behind the construction of the LAC was to maintain a modular concept throughout the manufacture: thus each subassembly was made and tested separately and all major subassemblies were interchangeable between detectors. Even when a detector had been filled with gas and sealed it was still possible to dismantle it and recover all the major components so that it could be reconstructed.

The choice of gas mixture was governed by the requirements for low background, moderate sensitivity to hard X-rays, and long life in orbit. The former consideration suggested that the amount of xenon in the mixture should be limited both to reduce the total Compton cross section and to reduce the number of escape events (Mason 1981). The choice of quench gas is determined by the requirement for a long reliable life. Methane is unsuitable where the radiation environment is unpredictable as is the case of a satellite in low earth orbit. High counting rates cause the methane to polymerise and form deposits on the anode wires, which can cause electrical breakdown and the eventual loss of the counter. The choice was thus made to use carbon dioxide

which requires much greater attention to gas purity, and electric field configuration, but has several orders of magnitude greater resistance to high counting rate induced polymerisation (Smith and Turner 1982). Good energy resolution depends on gas purity and on the design of the electrodes. Experience from Ariel V, Ariel VI and EXOSAT (Villa et al. 1976; Hall et al. 1981; Turner et al. 1981) shows that gas purity requires strict adherence to ultra high vacuum standards and materials in the construction of the counter.

The LAC was divided into eight detectors in order to keep the wires in the proportional counters short enough for their resonant frequency to be above the main spacecraft resonance (100 Hz), and to support the window and collimator against the internal pressure in the most efficient way (i.e. with least loss of effective area and lowest mass). Given the dimensions on the spacecraft side panel (90×130 cm), these considerations argued for a rectangular detector of about 60×20 cm. Once the interface to the spacecraft was fixed simple trade off studies showed that high internal pressure was more mass efficient than a deep detector, and that the optimum structure was a thin walled pressure vessel supported externally by ribs, with the window supported by the collimator against the internal pressure. An exploded view of the LAC detector is shown in figure 3a.

3.1.2. Detector housing

The detector body (see figure 3a) is made from thin (0.7 mm) stainless steel supported against the internal pressure by ribs of 1.5-mm stainless steel at 26-mm pitch; the internal dimensions are $560 \times 180 \times 57.3$ mm. The ultimate stress limit is 6 atm and each unit was tested to 4 atm (3 atm for fully assembled detectors). In order to maintain the cleanliness of the pressure vessel to UHV standards the detector bodies were heat treated and cleaned at several stages during manufacture.

3.1.3. Electrode structure

The aim of the electrode design was to achieve gain uniformity and to minimise saturation effects. Space charge saturation is more significant in carbon dioxide quenched mixtures, and causes departure from strict proportionality and degraded resolution. For this reason the gas gain is set as low as possible (2000) to minimise the number of positive ions, and the anode wire diameter is correspondingly large (40 μm) to decrease the space density in the avalanche. Variations in gain from place to place also degrade the overall resolution of the detector. Precise location of the wires and good surface quality are therefore essential. The square cathode cell design of the LAC (figure 3b) contributes to the gain uniformity because in this configuration the gain is least sensitive to anode position (Smith and Turner 1982).

The electrode is of modular construction being made up from four identical units comprising the anode and cathode wires for one layer (see figure 3b). The wires are all individually sprung and suspended between aluminium end bars. The anode wires have a diameter of 40 μm while the cathode wires are 50 μm. The material is stainless steel which can easily be crimped into the terminating tubes. The insulators are made from PTCFE (Kel-F), and the end veto strips (see section 3.1.7) are supported from the end bars with PTCFE pillars. Following optical inspection a single layer was clamped up together with three others to form a complete array, the wiring connections were made

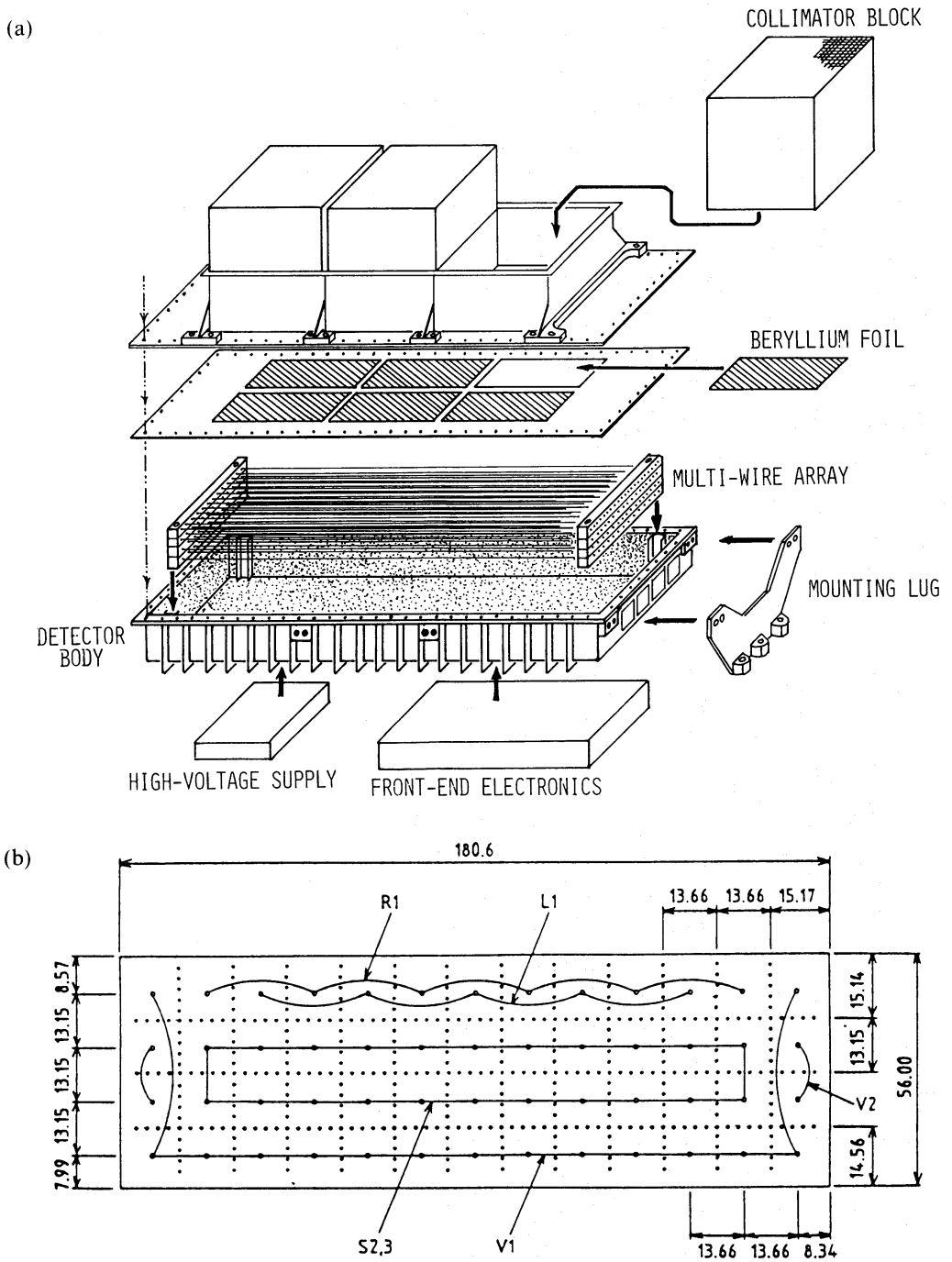

Fig. 3. (a) An exploded view of a LAC detector, showing the components.
(b) Cross section of the proportional counter gas cell showing the anode connections. Dimensions are in unit of mm.

and the assembly was vibrated to a specification higher than that applied to the complete detector. The array was then installed in a gas flow proportional counter and the gain uniformity was measured. Only those arrays having a uniformity better than 3% (peak to peak) were accepted for installation in the detector. The manufacture and all operations involving exposure of the array were carried out under clean conditions

since any dust particle adhering to the wires could cause electrical breakdown, and the wires are too delicate to clean post factum.

3.1.4. Entrance window

The beryllium window together with its seal to the detector body forms the closure to the pressure vessel. Its thickness determines the sensitivity of the LAC to soft X-rays; 62 μm was chosen to give reasonable freedom from leaks and adequate soft X-ray response. Leak free beryllium foil of this thickness was not available in a size sufficient to cover a detector with a single piece. Also the mis-match between the expansion coefficients of beryllium and the stainless steel body would have placed an unacceptably high stress on the seal if a single piece were used. A technique developed for Ariel VI solves this problem (Hall et al. 1981): a mosaic made up of 6 pieces of beryllium bonded into a thin (50 μm) stainless steel foil mask allows stress relief of the joint by flexure of the thin steel foil and enables smaller more reliably leak tight pieces of beryllium to be used. After the electrode had been inserted and tested the complete window mosaic was bonded on to the detector body using conductive epoxy. The window and its seal are supported against the internal gas pressure by the collimator assembly which was then bolted to the detector flange.

Once the detector had been sealed it was baked under vacuum at 100°C for 10 d, and then filled with the gas mixture. The gain was checked prior to final crimping of the filling tube, in order to ensure that all detectors had identical gain; small adjustments in pressure were made if required.

3.1.5. Collimator

The collimator field of view is a compromise between the requirement for a low diffuse X-ray flux and confusion limit, and the attitude control tolerance (see table 1). The more usual hexagon cell was divided in half to achieve the necessary elliptical field of view in a simple way. The choice of material (stainless steel) was based on mechanical stiffness, X-ray absorption and on thermal considerations (its low conductivity contributes to the thermal stability of the LAC under different solar exposure).

The collimators were assembled by hand with frequent checks for dimensional accuracy. Stainless steel sheets, 25 μm thick, were pressed to create cells with a semi hexagon cross section. Two formed sheets were bonded together with a plain sheet trapped between (figure 4); these subassemblies were then stacked to form a collimator block. The bottom 15 mm of the collimator was coated with silver paint to prevent contamination of the spectrum by iron K fluorescence. The individual blocks were optically evaluated and then measured in an X-ray beam to establish the transmission (80–85%) and the optical axis. Three blocks of collimator 158.5 mm square by 150 mm high were coaligned and bonded into the collimator housing of each detector (figure 3a). A final check of the optical axis of the complete detector, in a vacuum, was made using an X-ray beam. The measured field of view was $0.^{\circ}92 \times 1.^{\circ}78$ for a single detector; alignment errors increase the FWHM to $1.^{\circ}08 \times 2.^{\circ}0$ for the complete instrument.

3.1.6. Thermal foil

The thermal foil in front of the collimator is necessary to stabilise the thermal environment of the LAC. It was designed to be as thin as possible in order to minimise X-ray absorption. It is composed of 2 μm thick Mylar foil coated with aluminium on

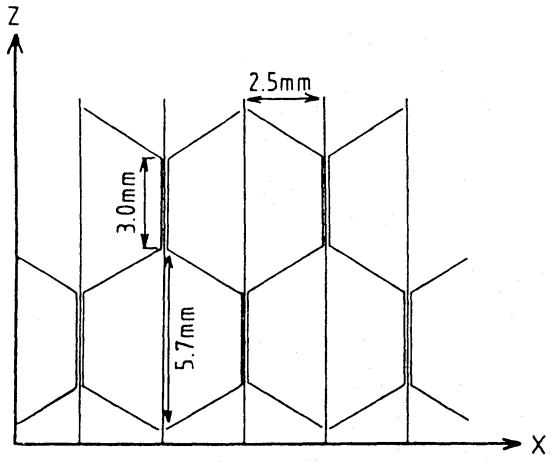

Fig. 4. Cross section of the collimator showing the shaped and flat plates.

both sides and an outer foil of 3 μm thick Kapton coated with aluminium on the inside. The total thickness of aluminium is 1000Å.

3.1.7. Background reduction

Background reduction was achieved in two ways: a highly efficient wall-less guard counter system was designed (Holt 1970; Peterson 1975; Culhane 1975); and great attention was given to shielding the detector volume from the diffuse cosmic X-ray background. Of the four layers of anodes shown in figure 3b, the back layer (V1) and the outer wires of the other layers (V2) formed three sides of the guard counter; the fourth and fifth sides are end guard cathodes (EV) similar to those used on EXOSAT (Bailey et al. 1978; Turner et al. 1981). The remaining wires (the signal anodes) were connected as shown in figure 3b. Alternate anodes in the front layer were connected to form two groups (L1 and R1) which were operated in mutual anticoincidence, and in anticoincidence with all other anodes including the guards. The signal anodes in layers 2 and 3 are effectively surrounded on all sides by guards so that mutual anticoincidence is less important; they are all connected together (S23 in figure 3b).

EXOSAT and Tenma experience shows that the diffuse cosmic X-rays become a dominant source of background in an unshielded detector that already has a highly efficient charged particle rejection system (Mason 1981; Koyama et al. 1984). For satellites in low earth orbit X-rays produced in the upper atmosphere are significant as well, and a further source of unwanted background comes from the X-ray sources outside the field of view of the collimator. The only way to remove this background is by shielding. The LAC is shielded with tin, 0.2 mm thick, placed either on the detector itself or on adjacent parts of the spacecraft so as to cover all directions other than the field of view of the collimator. The thickness of the tin is sufficient up to about 60 keV above which the background due to Compton interactions of gamma rays begins to dominate.

3.1.8. High voltage

Each LAC detector has its own high voltage (HV) supply, the output voltage range is set by fixed resistors but control from the main electronics allows 16 fine levels

between 1660 and 1960 V to be commanded in orbit for each individual detector supply. Transfer of the HV output to the distribution network uses a high specification Reynolds connector to facilitate replacement of faulty units if necessary. No potting is used on the high voltage distribution network and anode connections because of its inherent unreliability; the network components are however coated conformally to protect them from humidity and damage. The high voltage components were tested for tracking and breakdown at 3000 V (a comfortable margin over the operating voltage of 1830 V); the test level was set at <10 pulses per minute at a threshold of 2×10^{-16} C.

3.1.9. Calibration source

A motorised ^{109}Cd calibration source is mounted on the back of each detector opposite a small beryllium window. On command the stepper motor rotates through 90° and the source emerges from its tantalum shield to stimulate the detector with 22-keV X-rays.

3.1.10. Thermal expansion mountings

The mounting lugs joining the detectors to the spacecraft are of special design to hold each detector in alignment yet allow differential thermal expansion between the mainly aluminium spacecraft and the stainless steel detectors; the transmission of vibration from the spacecraft to the detectors is controlled by a damping device incorporated in the lugs.

3.2. Electronics and Data Handling

3.2.1. Signal processing

The configuration of the signal processing system of the LAC is illustrated in figure 5. The signals from each detector are first amplified and shaped by the front end electronics mounted on the detector; the shaped signals are then transferred to the main electronics which controls the event selection and converts the analogue pulses into digital form. The normal event selection criterion is

$$(\mathrm{L1}\,xor\,\mathrm{R1}\,xor\,\mathrm{S23})not(\mathrm{V1}\,or\,\mathrm{V2}\,or\,\mathrm{EV})\,.$$

These data are then further processed (e.g. by combining the data from several detectors), and edited into the telemetry format by the data processor.

3.2.2. Front end electronics

The front end electronics (FEE) contains individual charge sensitive preamplifiers and shaping amplifiers for each anode group; the end veto has in addition an inverting stage. Two FETs are used in parallel in the first stage of each preamplifier because of the high capacitance of the anodes in the large LAC detectors. The unipolar output signals from the FEE have an amplitude of 3 V, a risetime of 1 μs and a fall time of 2 μs.

3.2.3. Analog processing

In the main electronics there is a separate signal chain, anticoincidence logic and ADC for each detector. As shown in figure 5, the signals for each of the six anode groups, (L1, R1, S23, V1, V2, EV), go through pole-zero cancelation, shaping, and fine gain control, and then via a coarse gain amplifier and signal multiplexer to the ADC. The multiplexer (Input Select) allows signals from any anode group to be fed to the ADC for diagnostic purposes, although in normal operation only L1, R1 and S23 are

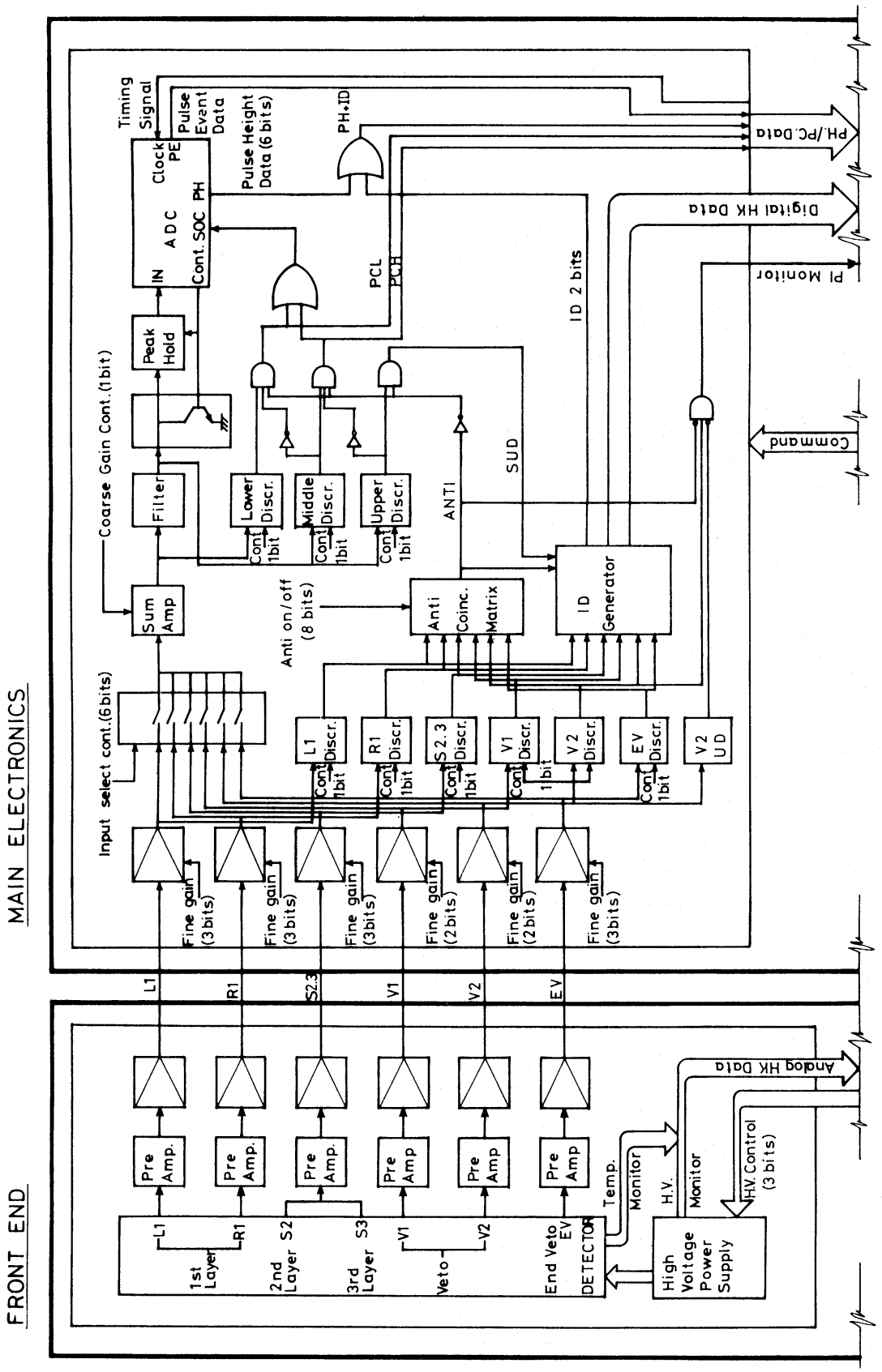

Fig. 5. The LAC signal processing scheme.

connected. Identification of the anode group (i.e. L1, R1 or S23) for each signal processed by the ADC is provided by a priority encoder incorporated in the anticoincidence logic.

The discriminators for the anticoincidence logic signals have two commandable levels (0.5/1.0 keV), which are separate from the lower discriminator for the main signal which also has two levels (0.8/1.2 keV). The coarse gain amplifier has two levels which allow the detector energy range to be set to either 0.5–37 keV or 0.25–18.7 keV by changing the whole energy range by factor of 1.98. The energy range can be extended further, e.g. to 70 keV, by changing the HV level; small changes to the HV level also serve to correct gain drifts in orbit due for example to gas leakage from a detector. More precise gain setting and alignment of the gains of the eight detectors is enabled by the fine gain control which has 8 steps of 2% width; it can be set independently for the three anode groups.

The ADC converts the signal amplitude into one of 64 channels and has a conversion time of 206 μs, this introduces significant dead time for bright sources.

3.2.4. Digital data processing

The digitised signals are passed to the data processor which has two main modes MPC and PC. In the MPC mode the 64 energy channels are compressed to 48 by combining in pairs the upper 32. The first 32 channels cover from 0 to 18.5 keV (0.58 keV/channel) and the remaining 16 channels 18.5 to 37.0 keV (1.16 keV/channel). There are three main sub modes: MPC1, 2 and 3. The characteristics of the data modes are described below and the details of each mode are given in table 2:

i) MPC1 mode: mainly used for spectral studies of faint sources. Events are accumulated in sixteen separate spectra of 48 channels each. The sixteen spectra comprise the top (L1 and R1) and middle (S23) layers from each of the eight detectors. The separation of top and middle layers improves the signal to noise ratio for weak sources and helps with background estimation.

ii) MPC2 mode: provides compression of the data by a factor of eight enabling better time resolution. It combines the top and middle layer spectra from four detectors into one and gives two separate spectra. The combination of layers decreases the signal to noise ratio and background estimation is less precise. It is suitable for sources stronger than 10 mCrab.

iii) MPC3 mode: carries this process further by combining the 48 energy channels into twelve and grouping all eight detectors together, giving a further factor of eight compression.

iv) PC mode: used for timing studies; it by-passes the ADC to avoid dead time effects. Signals are divided into two energy bands by three discriminators (lower, middle and upper) and no other energy information is retained. In this way the dead time is reduced to 16.5 μs per event and time resolution down to 976.6 μs ($=1/1024$ s) is obtained with two energy bands per detector group. The lower discriminator is the same as that used for the pulse height spectra, while the middle and upper discriminators have two commandable levels (see table 4) which can be set independently for the two groups of four detectors. This allows four (overlapping) energy bands to be selected. The lower band for each detector group is sampled twice as often as the upper to give the

Table 4. Energy (keV) of the discriminator levels.

Lever	CG-L		CG-H	
	H	L	H	L
Lower	1.53	1.19	0.77	0.60
Middle	15.7	5.67	7.94	2.86
Upper	24.3	17.9	12.3	9.05

Table 5. Source intensity causing overflow.

Mode	CG	Bit rate		
		High	Medium	Low
MPC1	H	12 Crab	0.8 Crab	0.2 Crab
	L	5	0.4	0.1
MPC2	H	24	1.6	0.4
	L	10	0.8	0.2
MPC3	H	24	1.6	0.4
	L	10	0.8	0.2
PC		4	0.5	0.1

maximum time resolution in the band with the greatest signal to noise ratio. The middle and upper discriminators do not affect the MPC modes.

3.2.5. Housekeeping

Most of the housekeeping parameters are not of interest to observers, being related to the health of the LAC and of the spacecraft. However some of the LAC housekeeping counting rates are important because they can be used to help with background estimation; these are the P. I. Monitor (PIM), the Surplus over Upper Discriminator (SUD) and the count rate of the radiation monitor (SOL2). The PIM monitors the counting rate of the V2 guard anodes (see figure 3b) in anticoincidence with the other anodes and with the upper level discriminator. This parameter approximates to the internal background, within the ADC range, of a single cell, since V2 is shielded by the LAC body from direct X-ray illumination. The SUD is the counting rate above the upper discriminator in anticoincidence with the guards, i.e. those X-ray-like events in the detector with an energy above 24 keV. This is useful in background normalisation (see section 5.1). The SOL2 monitors the local radiation environment and is used to turn off the LAC if the intensity gets too high. Because it has a thin Mylar window over a solid state detector it is sensitive to electrons. Therefore, it is used to determine the periods when electron flares occur which may disturb LAC observations.

3.2.6. Data recording and telemetry

The data from the MPC or PC modes are formatted together with the housekeeping in telemetry frames which are recorded on the BDR at one of three bit rates: 16 kbps, 2 kbps, and 512 bps. If the number of data events between successive

telemetry readouts becomes larger than 256, the telemetry word overflows and the true number of events is lost; the mode and bit rate have to be selected to avoid this. The maximum source intensity for which observations by the LAC are free from telemetry overflow is listed for each mode and telemetry rate in table 5. The overflow can in some cases be recovered (G. Hasinger 1988, private communication).

4. Calibration

The construction of LAC response function requires a knowledge of the linearity, energy resolution and efficiency, over the full energy range, as well as the uniformity of these quantities over the entire sensitive area. This information was derived from extensive ground calibration (Takano 1987) and from in-orbit observations of the Crab Nebula and Cas A.

4.1. Efficiency

The LAC efficiency as a function of energy was derived from technical data, such as the beryllium window thickness, gas composition and pressure; from measurements with X-ray beams performed prior to launch; and from observations of the Crab Nebula.

The mean transmission for each of the beryllium windows was found from its area and mass. The relation between these quantities and the X-ray transmission had previously been determined at several energies on selected windows covering the full range of thicknesses used in flight detectors. The results of these laboratory measurements of X-ray transmission were consistent with the mechanical properties and certified composition of the foil.

The efficiency calculated from the gas properties, detector dimensions and window thickness is modified by the effect of the anticoincidence; some X-ray events are rejected if they occur near the cell or layer boundaries. The loss is caused either when the primary electron cloud produced by an X-ray photon is shared between different cells or when a fluorescent X-ray photon from a gas atom is absorbed in another cell. This loss of X-rays is energy dependent and can be represented by an energy dependent dead region between cells and layers. The effective size of the dead region between cells was measured at 8, 20 and 30 keV by scanning a detector with a narrow X-ray beam of 0.5-mm diameter. From geometrical considerations, the size of the dead region (D) can be estimated as

$$D(\mathrm{mm}) = 0.45r(\mathrm{mm}) + 0.2\,,$$

where r denotes the mean free path of electrons. The measured results and the estimated curve are shown in figure 6. The measured ratio of the X-ray count rate with anticoincidence on and off is compared to the predictions of the model in figure 7. Since the agreement is good the dead region model is used to modify the calculated efficiency for the effect of anticoincidence.

Escape of fluorescent photons from the xenon and argon also modifies the response function by shifting down the detected energy. Pre-launch calibration showed that about

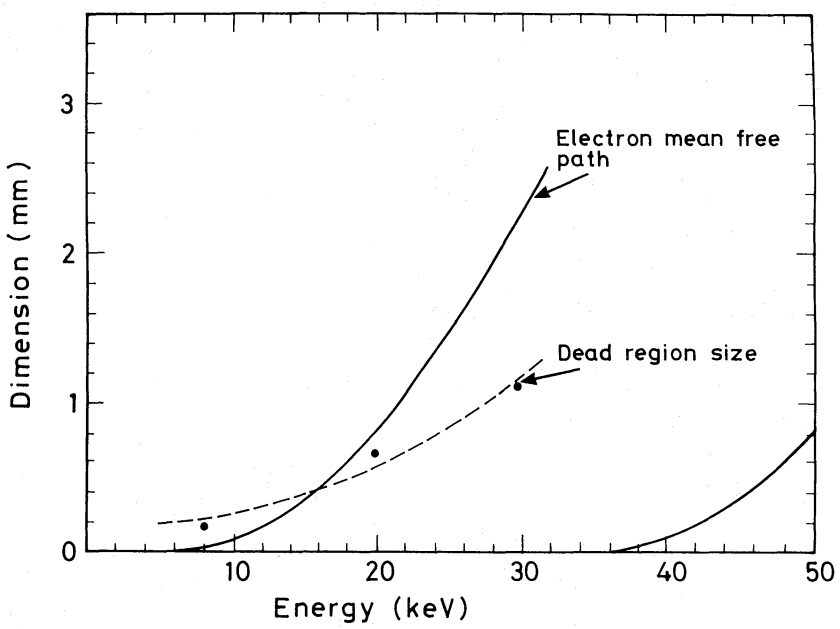

Fig. 6. The dimension of the dead region caused by inter-cell anticoincidence, as a function of energy. The points were measured using a narrow X-ray beam scanned across the cell boundaries, and the dashed curve is the model mentioned in the text. The solid line shows the electron mean free path.

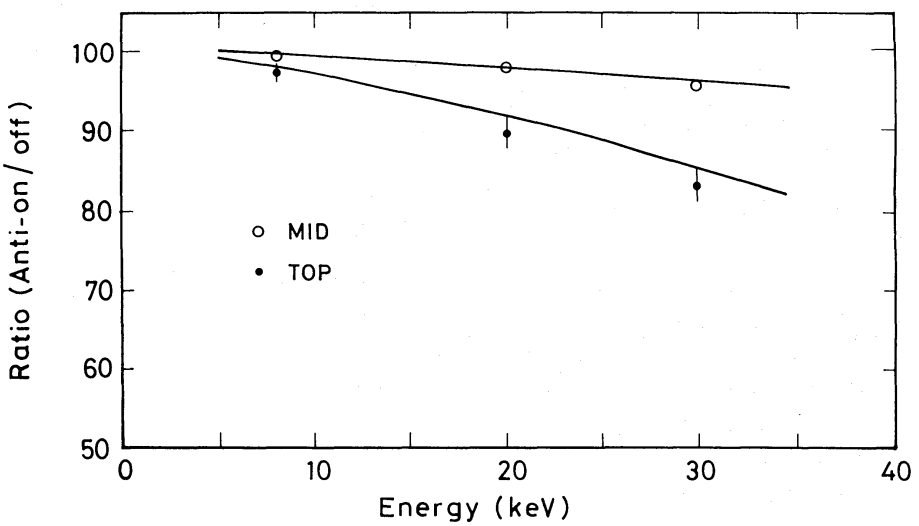

Fig. 7. The effect of anticoincidence on the count rate at different energies.

5% of the X-rays are affected in this way, however many of these are rejected by anticoincidence when the photon is absorbed in another layer or cell. A theoretical calculation, taking into account the measured anticoincidence rejection, showed that the effect is reduced to about 1.5%. This was included in the response function.

The final efficiency function was referred to the observed Crab Nebula spectrum (see section 4.4 and figure 8 below).

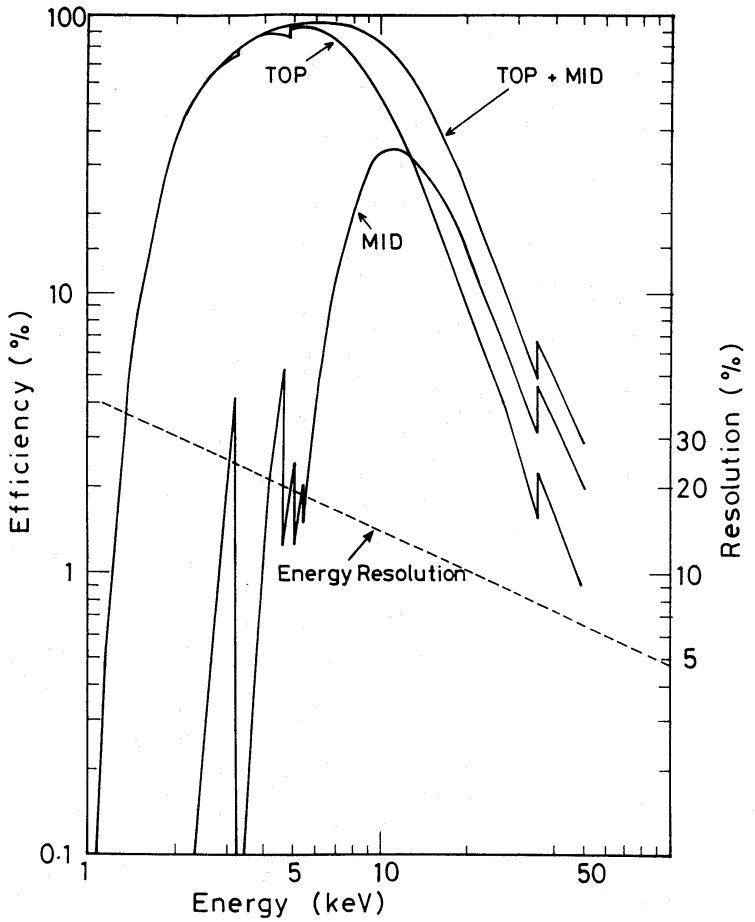

Fig. 8. The photopeak efficiency of the LAC for the top, middle, and top plus middle layers (solid curves) and the energy resolution (dashed line) as a function of energy. The measured energy resolution follows closely the functional form $E^{-0.5}$.

4.2. *Linearity*

The linearity and energy resolution were determined by irradiating the detectors with a broad parallel beam of monochromatic X-rays at several energies and measuring the pulse height distribution. An interesting feature of the resultant pulse amplitude versus photon energy curve, shown in figure 9, is the jump at the Xe L edge (4.8 keV) caused by the change of mean ionization energy of the gas (Carlson et al. 1966). This has been observed before in a xenon filled gas scintillation proportional counter (Koyama et al. 1984) and in an argon filled proportional counter (Jahoda and McCammon 1988). The xenon L edge linearity jump in the LAC (70 eV) is the same as that observed by Koyama et al. (1984); the effect at the Ar K edge (3.2 keV) is smaller than 10 eV.

The pulse amplitude shows saturation at high signal levels (figure 9). This is due to the space charge effect around the anode wires; it becomes more significant for higher gas gains. To check this feature the overall linearity (pulse amplitude vs X-ray energy) was measured for several high voltage levels. The result can be well approximated by the following quadratic expression (Takano 1987):

$$P = A + BE + CE^2 ,$$

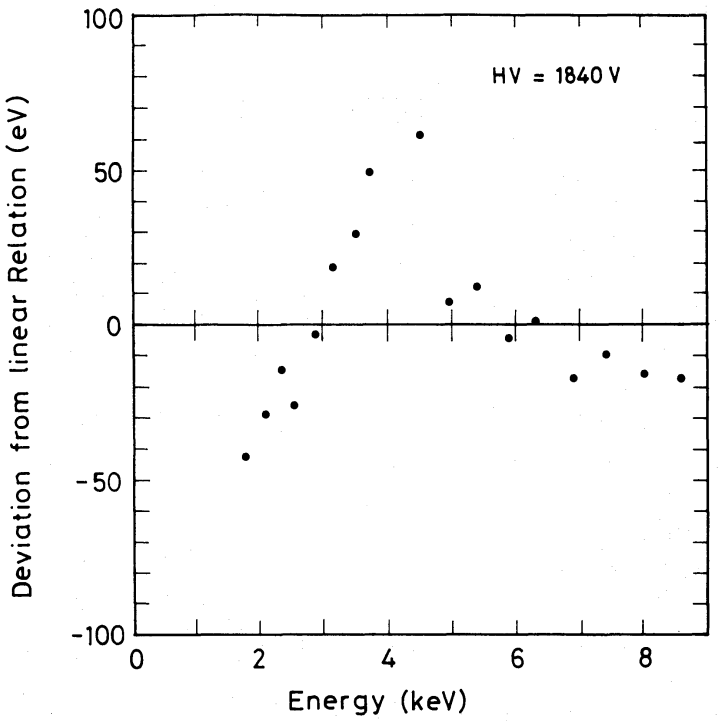

Fig. 9. The LAC pulse amplitude (shown as a deviation from the linear relationship) as a function of energy; the jump at 4.7 keV is the result of the change in mean ionisation energy of xenon above the L edge, there is some saturation at the higher energies.

where P denotes the pulse amplitude, E is the X-ray energy and A, B and C are constants. As shown in figure 10 the ratio C/B has an exponential dependence on the high voltage, i.e. it is proportional to the gas gain. This confirms that the observed pulse amplitude saturation is due to the space charge effect. The function fitted to the data in figure 10 was therefore used to correct the deviation from linearity of the LAC signals for all energies.

4.3. Energy Resolution

The energy resolution was measured using the broad beam measurements described above (section 4.2). In addition the gain uniformity, which determines the overall energy resolution of the detector, was measured by mapping each detector with a narrow beam of 8-keV X-rays. The results of these ground calibrations show that the overall resolution at 6 keV is 18% FWHM, with little deviation from the $E^{-0.5}$ dependence on energy predicted from theory (figure 8). The spectrum of Cas A observed by the LAC is shown in figure 11 fitted with a thermal bremsstrahlung model and an emission line. The fitted line energy is 6.63 ± 0.05 keV, which is consistent with the result obtained with the GSPC on Tenma (6.59 ± 0.02 keV; Tsunemi et al. 1986), and the results obtained by EXOSAT (Jensen et al. 1988). Thus the energy scale of the LAC is consistent with these instruments to 1%, and the combined energy resolution of the detectors in orbit is confirmed as 18.0% at 6 keV. Since the energy resolution in orbit is the same as measured prior to launch, the effect of temperature gradients within the detectors, caused by the zero-g environment, is negligible.

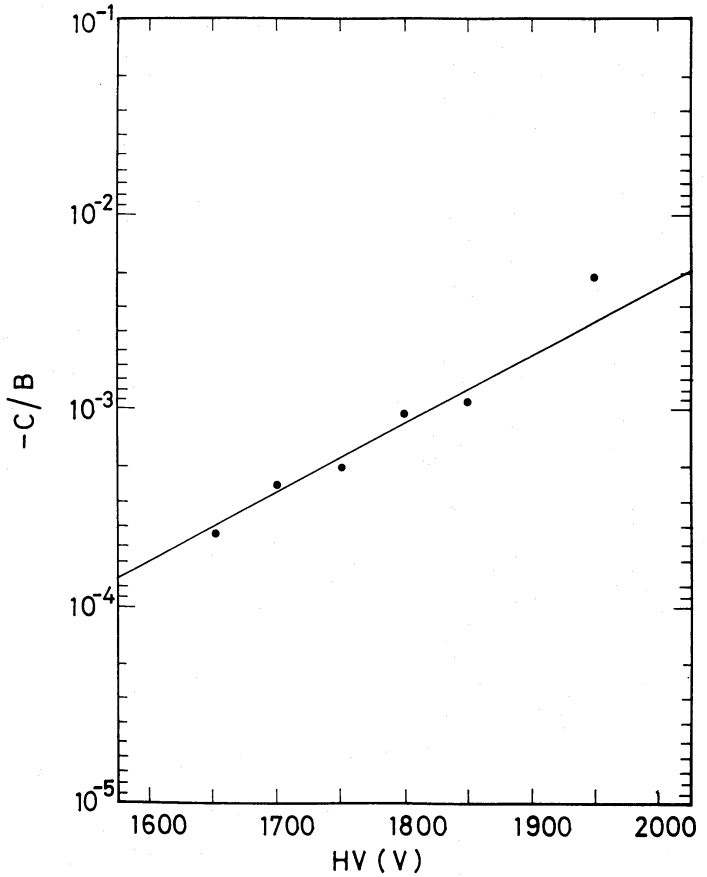

Fig. 10. Parameter describing space charge induced saturation of the pulse height at different high voltage settings.

4.4. *The Observed Crab Nebula Spectrum*

The efficiency and linearity of the detectors determined by the above calibration procedures were checked against the Crab Nebula spectrum measured with the LAC as shown in figure 12. The most significant discrepancy was an excess low energy absorption. A free fit to the observed Crab Nebula spectrum using the independently derived calibration requires that the neutral hydrogen column density (N_H) be $6 \times 10^{21}\,\mathrm{cm}^{-2}$ compared to the $3 \times 10^{21}\,\mathrm{cm}^{-2}$ generally accepted (Toor and Seward 1974; Charles et al. 1979; Schattenburg and Canizares 1986) using the cross sections by Morrison and McCammon (1983). This is well outside the errors in the ground calibration and in particular the expected error in beryllium window thickness. (It would require an underestimate close to a factor of two.) So far we have been unable to arrive at a satisfactory explanation for this excess absorption. For present purposes it can be approximated by assuming a larger beryllium thickness, and this has been incorporated in the calibration.

Using the calibration derived above a free fit to the Crab spectrum above 7 keV, where N_H uncertainties and collimator reflectivity (see below) are negligible, gives a power law of $9.15(\pm 0.5)E^{-2.08\pm0.03}$. This is sufficiently close to the Toor and Seward (1974) value of $9.7(\pm 1.0)E^{-2.1\pm0.03}$ for the calibration to be left unmodified.

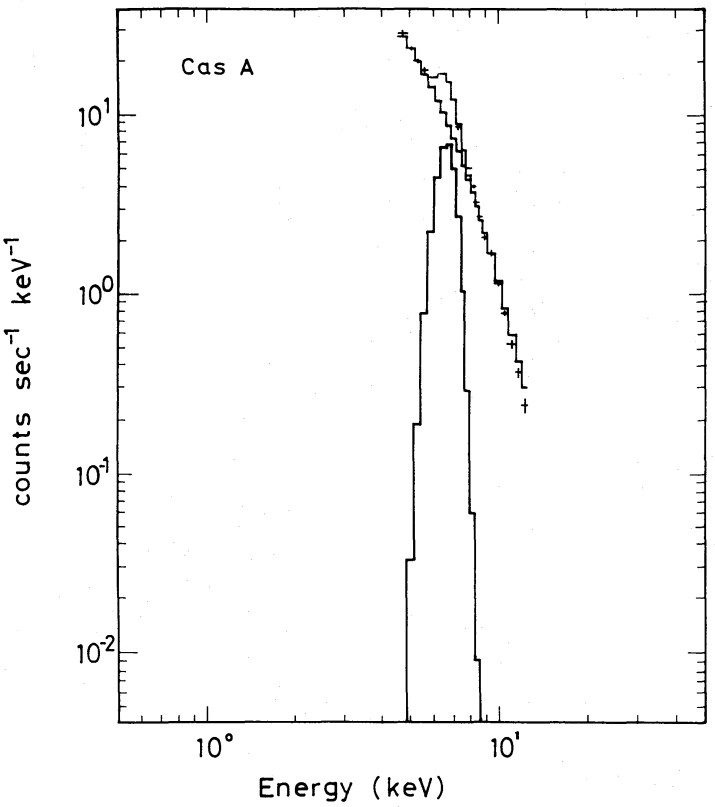

Fig. 11. The spectrum of the supernova remnant Cas A, observed with the LAC. The agreement between the data and the fitted spectrum (iron line energy 6.63 keV) demonstrates the accuracy of the energy scale of the LAC.

The Crab Nebula spectrum observed with the LAC, as shown in figure 12, is fitted using the calibration and corrections described above. The parameters of the Crab Nebula spectrum as measured by the LAC using the current calibration are shown in table 6.

4.5. Collimator Angular Response Function

The two dimensional collimator response was measured by slewing the field of view over the Crab Nebula at various elevation angles (Kondo 1988). The FWHM field of view and the offset of the optical axis from the satellite *Y* axis are shown in table 7 for the eight individual detectors and for their sum. The two dimensional overall response is shown in contours in figure 13.

The inner surfaces of the collimator are somewhat reflective to X-rays below 6 keV, but only to those inclined in a direction parallel to the slew plane (the shorter axis of the field of view). This is because the plates dividing the hexagons in half (see section 3.1.5) have a different surface finish from the rest. An X-ray source 2° offset from the field center in the slew direction (i.e. 1° outside of the nominal field of view) gives a few percent of the reflected X-ray flux. An offset angle of more than 3° is required to eliminate this contamination completely.

A more important effect of this reflectivity occurs in spectral determination. A source within the field of view but offset from the centre in the direction of the slew

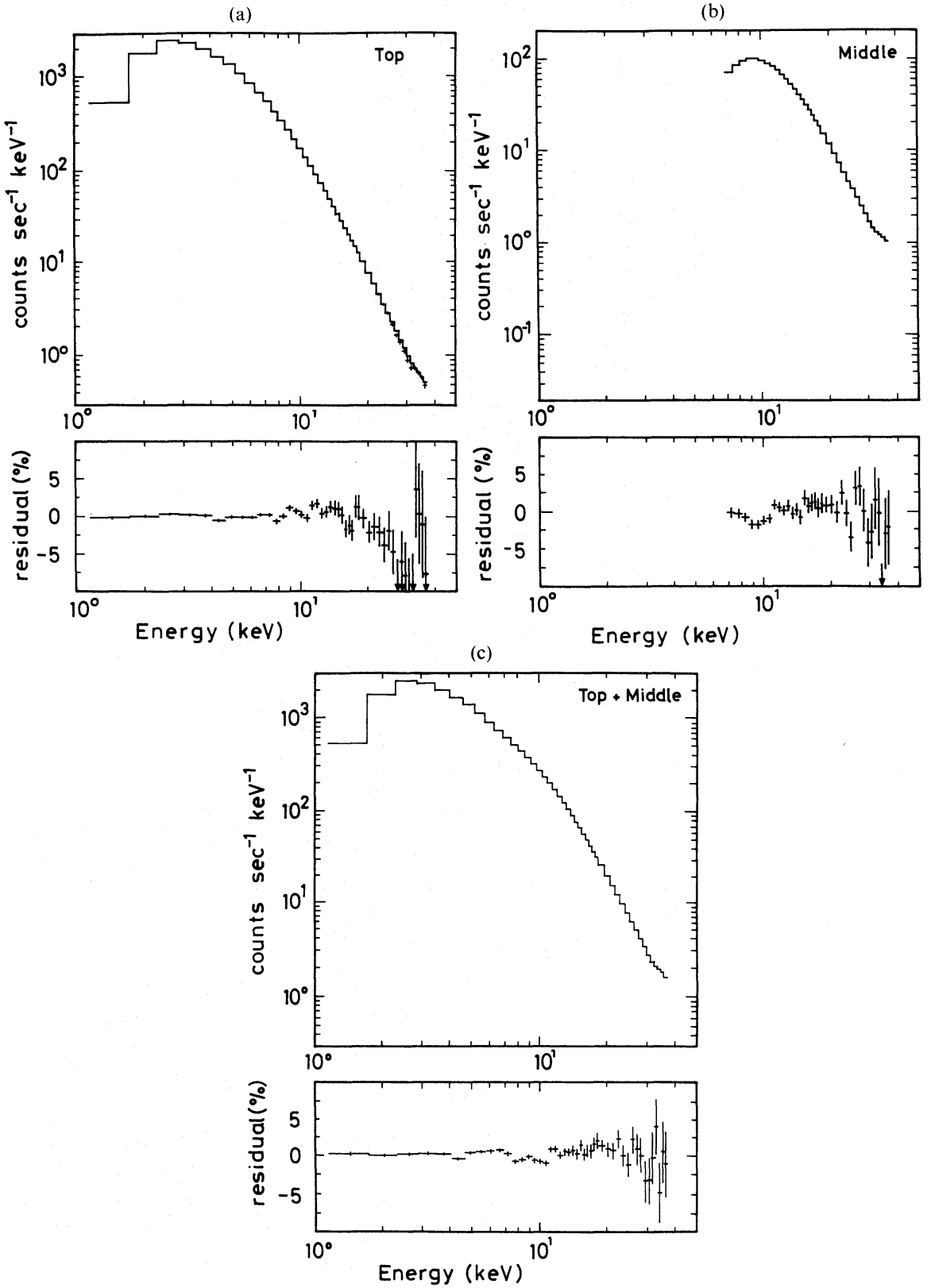

Fig. 12. The Crab spectrum observed by the LAC in (a) top, (b) middle, and (c) top plus middle layers, respectively. The parameters are given in table 6. The residuals (inset) are less than 2% in the energy range below 20 keV.

Table 6. Fitting parameters for Crab Nebula spectrum.

N_H	Photon index
$(3.2\pm0.7)\times10^{21}$ cm^{-2}	2.08 ± 0.03

Table 7. Collimator properties.

Detector	Offset angle*		FWHM field of view	
	Azimuth	Elevation	Azimuth	Elevation
S0	−0.18	−0.13	1.00	2.00
S1	−0.23	−0.12	1.08	1.95
S2	−0.12	−0.08	1.11	2.02
S3	−0.21	0.0	1.11	2.00
S4	−0.24	−0.09	1.08	1.99
S5	−0.24	−0.13	1.09	2.00
S6	−0.29	−0.07	1.09	1.96
S7	−0.27	−0.08	0.99	2.05
Overall	−0.224	−0.08	1.08	2.00

* Measured from the Y axis of the satellite.

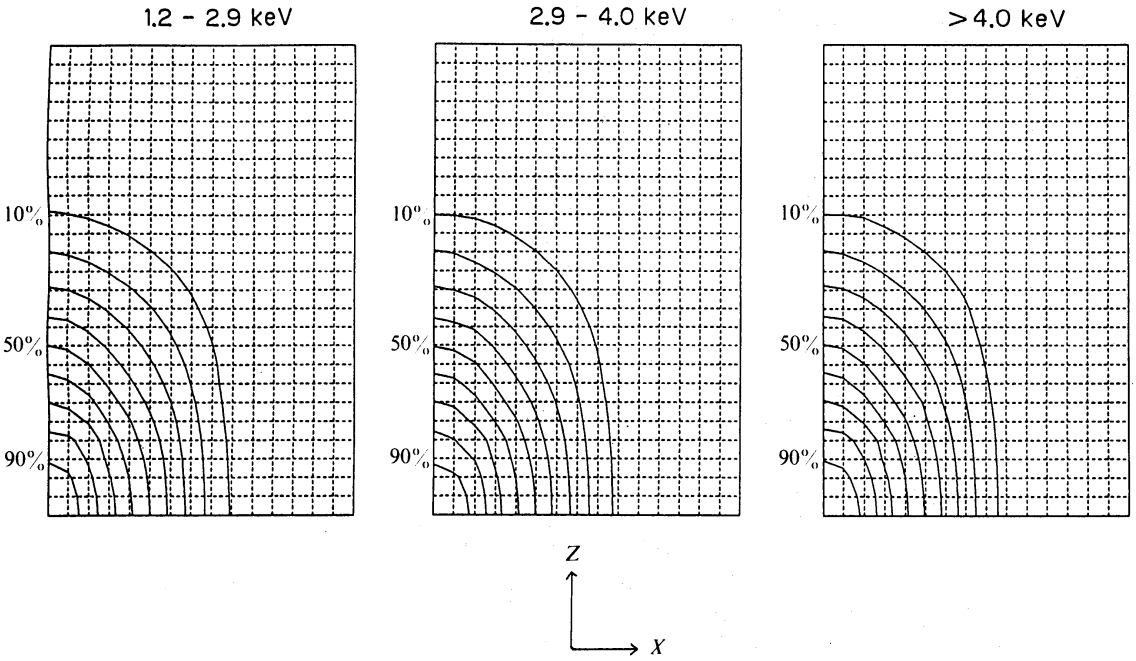

Fig. 13. The collimator angular response function. The grid size with dotted lines is 0°.1, and three different energy bands are shown. In the softer bands the effect of reflection modifies the contours by a few percent.

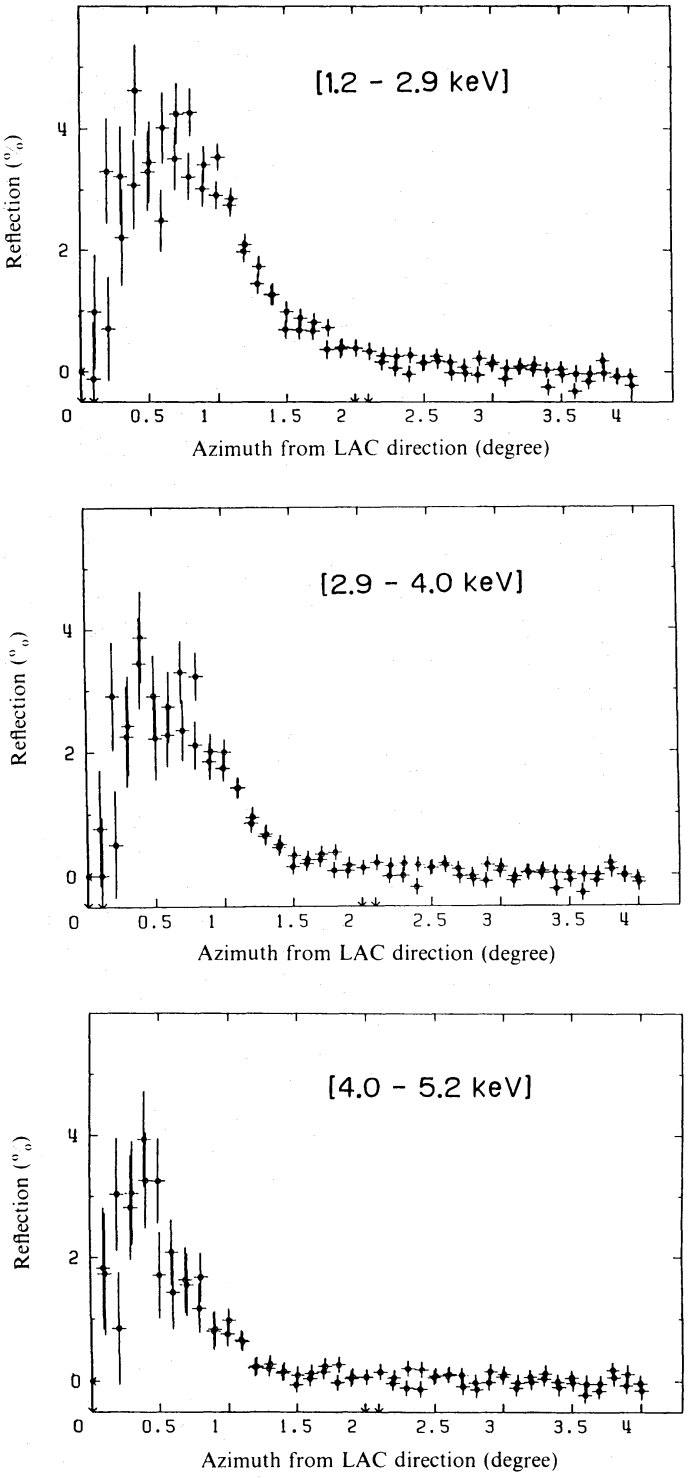

Fig. 14. The reflection effect in three energy bands from 1.2 to 5.2 keV, shown as a percentage of the *on*-axis flux, as a function of offset angle in the slew (Y) direction.

plane, will generate additional flux below 6 keV (the iron K edge). This has to be taken into account in fitting the spectrum. The amount of the reflection measured for the Crab Nebula is shown in figure 14 for three energy bands. It amounts to a few percent

for sources within 0°.3 of the optical axis.

5. Sensitivity

The sensitivity of the LAC is primarily limited by systematic and confusion errors because of the large effective area and the long observations. For faint sources systematic background subtraction errors dominate. For bright sources the collimator reflectivity and the limited accuracy of the calibration are often important. The calculation of the ultimate sensitivity of the LAC depends on a knowledge of these factors. Reflectivity and calibration have already been mentioned; the following sections deal briefly with the estimation of the internal background of the LAC and the effect of fluctuations in the diffuse background on source flux estimation. A more detailed discussion of these matters appears in the accompanying paper (Hayashida et al. 1989). The last section discusses the sensitivity based on these considerations.

5.1. Internal Background Estimation

The background counting rate measured when the LAC is pointed at the dark earth is about 50 counts s^{-1} (3.5×10^{-4} counts $cm^{-2} s^{-1} keV^{-1}$ over 1–37 keV) for the sum of the top and the middle layers. This rate increases by a factor of about 20 without the anticoincidence. In addition when the LAC observes a blank sky region the count rate increases by 18 counts s^{-1} due to the diffuse X-ray background within the collimator field of view. Because of the 31° orbital inclination, the residual non X-ray background varies by a factor of two round the orbit and through the observing day; very large increases are observed in the vicinity of the South Atlantic Anomaly (SAA) and smaller ones at high geomagnetic latitudes where the cosmic ray rigidity is reduced. Figure 15 shows the background count rate as a function of time for a complete day of fifteen orbits. The gaps in the data occur when the LAC is turned off for passage through the SAA, and other high background regions. When the LAC points at the Earth the decrease in count rate due to the screening of the diffuse X-ray background is noticeable.

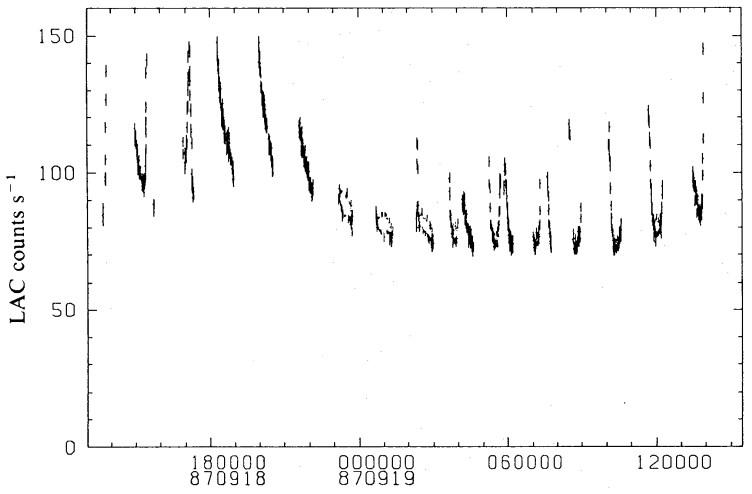

Fig. 15. The variation of the LAC counting rate (1–37 keV) during an observing day, with the detector field of view in a source-free sky.

Table 8. Identified half lives of radioactivity.

~8 hr	2500 ± 200 s	330 ± 30 s

Although the LAC is turned off during SAA passage the effect persists for some time after emergence. This is due to radioactive isotopes created in the material of the spacecraft and of the LAC itself, by protons in the SAA. Decay of these isotopes generates additional background in the LAC by means of Compton interactions of nuclear gamma rays. It varies in a complex way with time, depending on the length and altitude of the SAA immersion, and the time elapsed since. Ginga passes through the SAA on eight of the fifteen orbits each day, so the radioactivity builds up during these orbits and decays during the remaining seven. Table 8 shows the half lives identified in the data, however the time variability of the background is complex and several other decay times probably contribute (see Hayashida et al. 1989). The nature of the isotopes is difficult to determine; iron is the most abundant element surrounding the LAC, and it would be reasonable to infer that iron isotopes make a major contribution. However iron is intrinsically no more likely to become radioactive than the other elements making up the spacecraft; further study of the background is necessary to establish the most likely contributors. Because of the orbital eccentricity the altitude of the satellite during its passage through the SAA varies with the argument of perigee at a period of 37 days; this period is also observable in the secular variation of the LAC background.

In addition to the changes in total background count rate detailed above, changes in the relative contributions of the various background mechanisms through the day result in corresponding changes in the spectrum of the residual internal background. This makes the task of background estimation more difficult.

It is at present standard practice to devote one day, adjacent to the source observation, to an observation of nearby blank sky. The background so measured can then be used to generate an estimate of the internal background during the source observation. This estimation problem is complex: the background at any particular time of day, i.e. orbit number and position in the orbit, may be expected to be approximately the same on two successive days, however small fluctuations in the local radiation environment will take place from day to day, and long term trends (e.g. the 37-d variation) may have a nonnegligible effect. In some cases it has proved sufficient to restrict the source observation to a particular time of day when the background is low and stable, using as a background estimate the data taken from the same time interval on an adjacent day, normalised using the SUD count rate (see section 3.2). A more complex method divides the source and background observations, still for a selected time of day, into narrow ranges of SUD values. The source and background spectra within these ranges are separately accumulated and normalised. This method attempts to take into account the spectral changes in the background.

Neither of these methods is completely successful, in particular the spectral features in the background spectrum at 3 and 5 keV (figure 16) are difficult to reproduce accurately. Significant improvements in background estimation can be made using

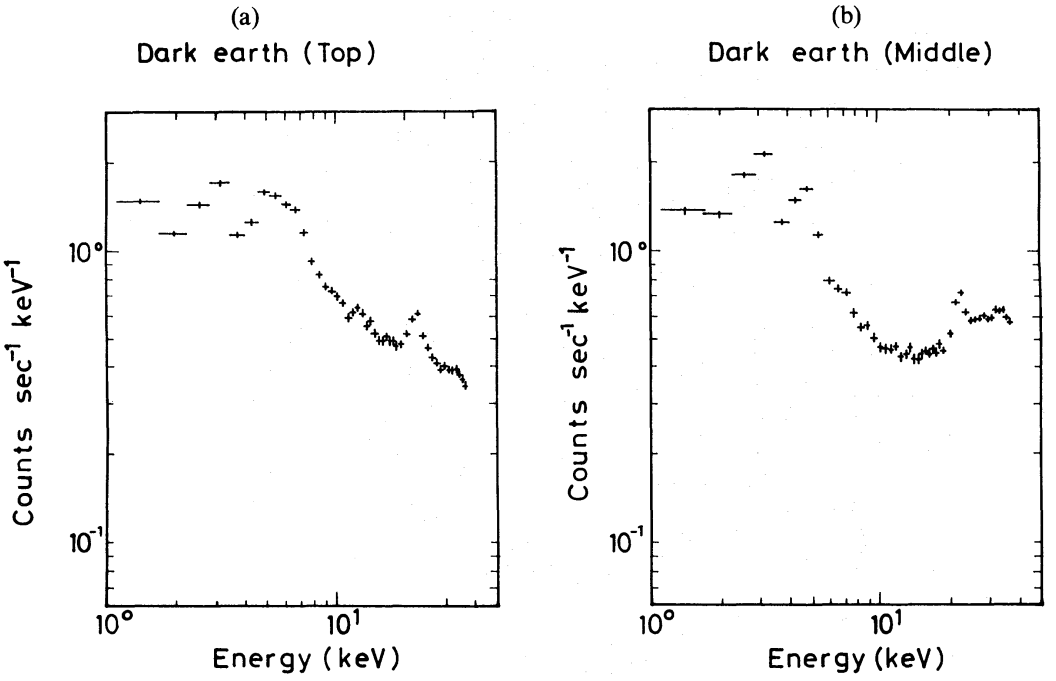

Fig. 16. The raw pulse height spectra of the non X-ray background (dark earth) for the (a) top and the (b) middle layers. Line-like features exist at 3 and 5 keV. The line at 22 keV is produced by the silver paint on the collimator.

modelling. This approach fits the intensity in each spectral channel as a function of time with a model polynomial whose parameters are related to the instantaneous radiation field (SUD, PIM and SOL2), the local geomagnetic field, the induced radioactivity, etc. The coefficients derived from a fit to the background observation are then used to estimate the background during the source observation. In addition to the improvement in spectral observations this method is also useful in timing observations when accurate background subtraction is needed throughout the day.

These methods are detailed, together with others, in Hayashida et al. (1989) and in general achieve a residual background error better than 0.02 counts s^{-1} in any spectral channel (1σ equivalent). To demonstrate the spectral capability of the LAC, the pulse-height spectrum of the Galactic ridge (~ 5 mCrab intensity) in a region $l \sim 3°$ and $b \sim -2°$ is shown in figure 17. The intense iron emission line discovered by Koyama et al. (1986) is clearly seen.

5.2. *Diffuse Background*

The diffuse background within the field of view of the LAC is 18 counts s^{-1} over the full energy range; fluctuations in this value from point to point on the sky will contribute to the error in the background estimate because source and background pointings are of necessity different. The size of the fluctuations can be predicted for the LAC field of view from a source number-flux relationship such as that derived by Piccinotti et al. (1982). This gives a 1σ equivalent fluctuation on the integrated diffuse background count rate of about 0.7 counts s^{-1} in 2–10 keV. In principle the fluctuations can be measured by pointing at many different blank sky regions and subtracting the internal background using one of the methods outlined above. Preliminary results from this procedure support the theoretical value (see Hayashida et al. 1989).

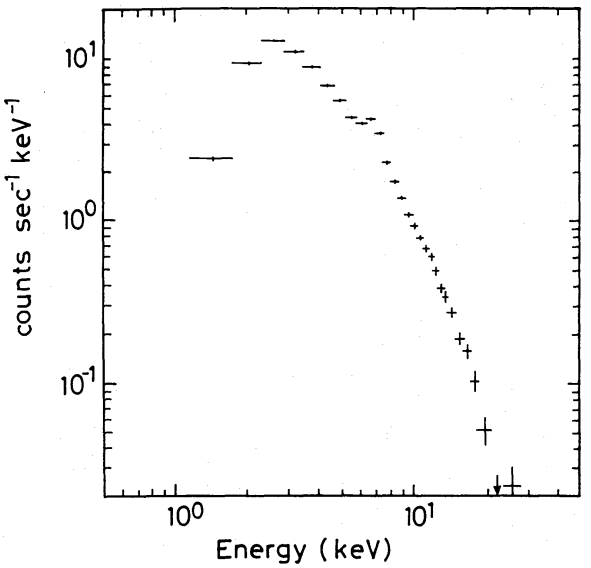

Fig. 17. The pulse height spectrum of the Galactic ridge emission observed with the LAC for the sum of top and middle layers. The intense iron emission line discovered by Koyama et al. (1986) is recognized.

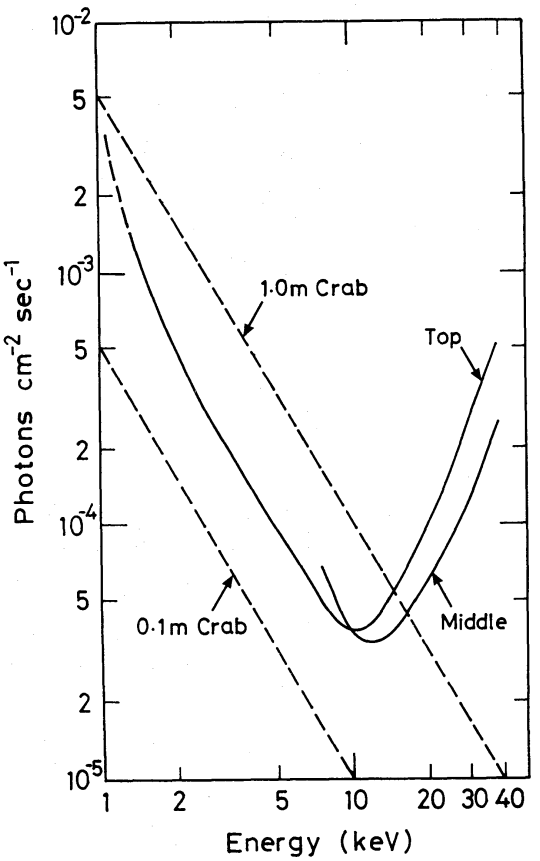

Fig. 18. The 3σ sensitivity of the LAC as a function of energy for top and middle layers. The dashed lines show incident spectra for a power-law photon index of 1.7 with intensities of 1 mCrab and 0.1 mCrab.

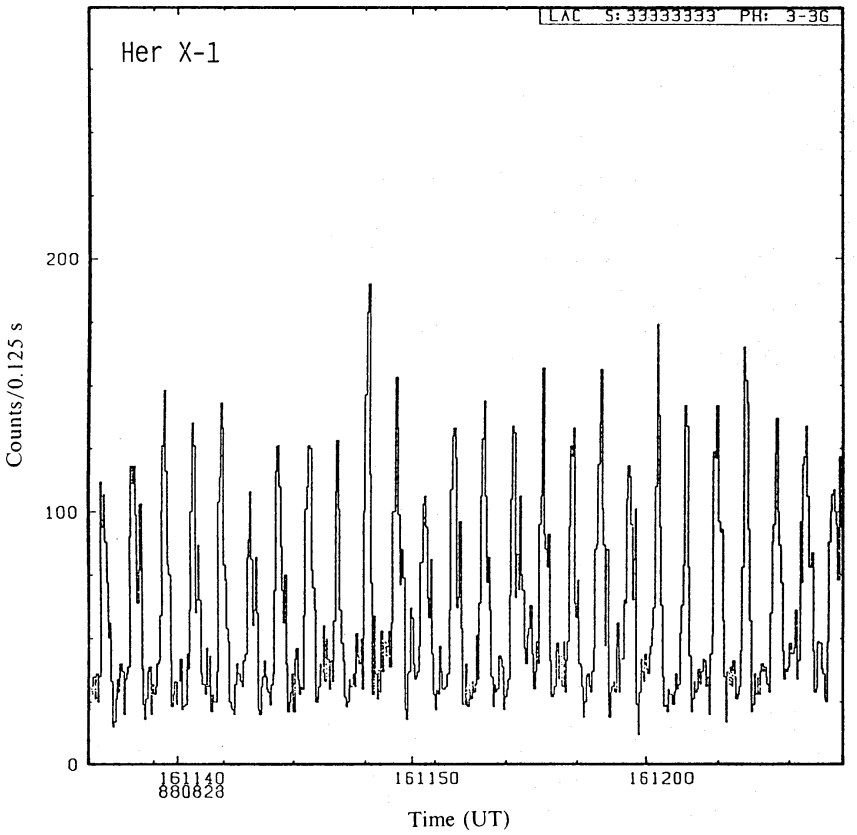

Fig. 19. The raw count rate of the LAC for an X-ray pulsar Her X-1 with 0.125-s bin. The source intensity is roughly 100 mCrab, and the individual 1.24-s pulse profiles are clearly seen.

5.3. *Sensitivity Calculation*

The sensitivity of the LAC for spectral measurements on weak sources, calculated using the errors derived above, is displayed in figure 18 as a function of energy. Since the errors are mainly systematic the integration time is not important; the sensitivities shown are calculated for a source observation time of 10000 s which is approximately the amount of low background data available in one day.

The large area of the LAC makes it particularly suitable for timing studies. In this case, where the absolute flux is not important, systematic effects are less significant and the statistical limits can be used. Figure 19 is an example of the raw count data of the LAC showing the individual profiles of the 1.24-s pulses of Her X-1.

The authors are grateful to Professors M. Oda, K. A. Pounds, Y. Tanaka and F. Makino and Dr. M. Cruise for their support and encouragement during the course of this major international collaboration. The LAC is the result of years of hard and dedicated effort by many scientists, engineers and technicians who have worked on both sides of the Earth in universities and in industry. Particular thanks are due to A. A. Wells, J. E. Spragg, A. J. Larrad, M. Waterman, A. S. Rate, C. H. Whitford, J. R. Dowson, A. Keith, M. Trower, and I. M. Mason, in the UK, and to T. Murakami, K. Yamashita, F. Nagase, H. Kunieda, H. Tsunemi, and S. Kitamoto in Japan. We

acknowledge particular contributions from our industrial partners: New Town Engineering (E. Kennedy), SIRA (J. Andrews), Electrofusion Corporation (W. J. Marcellin), and Meisei Electronics (K. Taguchi, K. Tanimoto, K. Sugiyama and T. Ishizuka). Financial support was provided by the Science and Engineering Research Council in the UK and a Grant-in-aid for Overseas Research by the Ministry of Education, Science, and Culture of Japan. Finally we thank Professor H. Matsuo and the ISAS launch team who successfully placed Ginga in orbit.

References

Bailey, T. A., Smith, A., and Turner, M. J. L. 1978, *Nucl. Instrum. Methods*, **155**, 177.
Carlson, T. A., Hunt, W. E., and Krause, M. O. 1966, *Phys. Rev.*, **151**, 41.
Charles, P. A., Kahn, S. M., Bowyer, S., Blissett, R. J., Culhane, J. L., Cruise, A. M., and Garmire, G. 1979, *Astrophys. J. Letters*, **230**, L83.
Culhane, J. L. 1975, *Vistas Astron.*, **19**, 1.
Hall, R., Ricketts, M. J., Page, C. G., and Pounds, K. A. 1981, *Space Sci. Rev.*, **30**, 47.
Hayashida, K., Inoue, H., Koyama, K., Awaki, H., Takano, S., Tawara, Y., Williams, O. R., Denby, M., Stewart, G. C., Turner, M. J. L., Makishima, K., and Ohashi, T. 1989, *Publ. Astron. Soc. Japan*, **41**, 373.
Holt, S. S. 1970, in *Introduction to Experimental Techniques of High-Energy Astrophysics*, ed. H. Ögelman and J. R. Wayland, NASA SP-243 (Scientific and Technical Information Division, NASA, Washington, D. C.), p. 63.
Jahoda, K., and McCammon, D. 1988, *Nucl. Instrum. Methods Phys. Res. Sect. A*, **272**, 800.
Jensen, F., Smith, A., Bleeker, J. A. M., de Korte, P. A. J., Peacock, A., and White, N. E. 1988, *Astrophys. J.*, **331**, 949.
Kondo, H. 1988, Master Thesis, The University of Tokyo (in Japanese).
Koyama, K., Ikegami, T., Inoue, H., Kawai, N., Makishima, K., Matsuoka, M., Mitsuda, K., Murakami, T., Ogawara, Y., Ohashi, T., Suzuki, K., Tanaka, Y., Waki, I., and Fenimore, E E. 1984, *Publ. Astron. Soc. Japan*, **36**, 659.
Koyama, K., Makishima, K., Tanaka, Y., and Tsunemi, H. 1986, *Publ. Astron. Soc. Japan*, **38**, 121.
Makino, F., and the ASTRO-C team 1987, *Astrophys. Letters Commun.*, **25**, 223.
Mason, I. M. 1981, Ph. D. Thesis, Mullard Space Science Laboratory, University College London.
Morrison, R., and McCammon, D. 1983, *Astrophys. J.*, **270**, 119.
Peterson, L. E. 1975, *Ann. Rev. Astron. Astrophys.*, **13**, 423.
Piccinotti, G., Mushotzky, R. F., Boldt, E. A., Holt, S. S., Marshall, F. E., Serlemitsos, P. J., and Shafer, R. A. 1982, *Astrophys. J.*, **253**, 485.
Schattenburg, M. L., and Canizares, C. R. 1986, *Astrophys. J.*, **301**, 759.
Smith, A., and Turner, M. J. L. 1982, *Nucl. Instrum. Methods Phys. Res.*, **192**, 475.
Takano, S. 1987, Master Thesis, The University of Tokyo (in Japanese).
Toor, A., and Seward, F. D. 1974, *Astron, J.*, **79**, 995.
Tsunemi, H., Yamashita, K., Masai, K., Hayakawa, S., and Koyama, K. 1986, *Astrophys. J.*, **306**, 248.
Turner, M. J. L., Smith, A., and Zimmermann, H. U. 1981, *Space Sci. Rev.*, **30**, 513.
Villa, G., Page, C. G., Turner, M. J. L., Cooke, B. A., Ricketts, M. J., Pounds, K. A., and Adams, D. J. 1976, *Monthly Notices Roy. Astron Soc.*, **176**, 609.